# Chemistry of [Cp*Rh($\mu$-Cl)]$_2$ and Its Dioxygen and Nitrosobenzene Insertion Products

**David W. Hoard and Paul R. Sharp***

Department of Chemistry, University of Missouri—Columbia, Columbia, Missouri 65211

*Received August 21, 1992*

Treating [Cp*Rh($\mu$-Cl)Cl]$_2$ (Cp* = $C_5Me_5$ = pentamethylcyclopentadienyl) with excess Na(Hg) (0.4%) in $CH_2Cl_2$ gives deep blue [Cp*Rh($\mu$-Cl)]$_2$ (**1**). Crystals of **1** from toluene/petroleum ether are monoclinic (*C*2/*c*) with $a = 33.068(8)$ Å, $b = 13.173(3)$ Å, $c = 16.810(4)$ Å, $\beta = 117.77(2)°$, $V = 6479.4$ Å$^3$, and $Z = 12$. The structure consists of two independent, nearly identical molecules (one on a 2-fold axis and the other in a general position) with short Rh–Rh bonds (2.623 Å average), bridging chlorides, and $\eta^5$-Cp* ligands. Methylene chloride solutions of **1** react rapidly with dioxygen at temperatures slightly above –78 °C to give an unstable (above ca. –15 °C in $CD_2Cl_2$) unsymmetrical, dioxygen adduct [(Cp*Rh)$_2$($\mu$-Cl)(Cl)($\mu$,$\eta^1$:$\eta^2$-$O_2$)] (**2**). Complex **2** is fluxional on the NMR time scale. The addition of $PPh_3$ to cold solutions of **2** gives Cp*RhCl$_2$(PPh$_3$) and the unstable (above ca. 0 °C in $CD_2Cl_2$) complex Cp*Rh(O$_2$)(PPh$_3$) (**3**). With excess PMe$_3$, **2** gives the fulvene complex [($\eta^4$-$C_5Me_4CH_2$)Rh(PMe$_3$)$_3$]Cl (**4**). Crystals of **4** from $CH_2Cl_2$/petroleum ether are monoclinic (*C*2/*c*) with $a = 16.618(5)$ Å, $b = 12.074(6)$ Å, $c = 27.319(7)$ Å, $\beta = 99.04(2)°$, $V = 5413$ Å$^3$, and $Z = 8$. Treating **1** with PhNO at 22 °C gives [(Cp*Rh)$_2$($\mu$-Cl)(Cl)($\mu$,$\eta^1$:$\eta^2$-PhNO)] (**5**) which, by NMR and a crystal structure determination, has a structure similar to that proposed for **2**. Crystals of **5** from toluene/hexane are triclinic ($P\bar{1}$) with $a = 9.290(3)$ Å, $b = 17.830(3)$ Å, $c = 8.941(3)$ Å, $\alpha = 92.60(2)°$, $\beta = 110.87(3)°$, $\gamma = 104.36(2)°$, $V = 1325.9$ Å$^3$, and $Z = 2$. The structure consists of an $\eta^1$:$\eta^2$-bound PhNO ligand (bridging the two $\eta^5$-Cp*Rh centers via the nitrogen atom), a bridging Cl, and a terminal Cl bound to the $\eta^1$-Rh center. A chloride ion is removed from **5** with TlBF$_4$ to give the first $\mu$,$\eta^2$:$\eta^2$-nitrosobenzene complex, [(Cp*Rh)$_2$($\mu$-Cl)($\mu$,$\eta^2$:$\eta^2$-PhNO)]BF$_4$ (**6**). Crystals of **6** from $CH_2Cl_2$/petroleum ether are monoclinic ($P2_1/c$) with $a = 10.933(4)$ Å, $b = 15.166(6)$ Å, $c = 18.136(10)$ Å, $\beta = 95.33(4)°$, $V = 2994$ Å$^3$, and $Z = 4$. The Na/Hg reduction of **5** in the presence of PhNO and TlBF$_4$ gives [Cp*Rh($\mu$,$\eta^1$:$\eta^2$-PhNO)]$_2$ (**7**). Treating the nitrosobenzene complexes with CO gives up to 35% yields of PhNCO.

## Introduction

The activation of molecular oxygen by late-transition-metal surfaces is a critical step in many catalytic reactions. Evidence indicates that activation occurs through dissociative adsorption with the formation of oxygen adatoms (Scheme I).[1] The analogous homogeneous solution process, dissociation of dioxygen into oxo complexes, is unknown for late-transition-metal systems[2] and is relatively rare for early-transition-metal systems.[3] As part of our efforts to develop the solution chemistry analogous to the surface chemistry, we have been exploring the synthesis and chemistry of late-transition-metal oxo and imido complexes[4] and we have now begun investigating the reactions of $O_2$ and RNO with multimetallic centers. Our goal is to prepare new bridging dioxygen and nitrosobenzene complexes of type A, B, and C (Scheme II) and, ultimately, to split the heteroatom–heteroatom bond to produce oxo and/or imido complexes. In this paper we describe successful syntheses of bridging dioxygen and nitrosobenzene complexes of type A and B from a reactive Rh(II) dimer and their structural and chemical characterization.[5]

### Scheme I

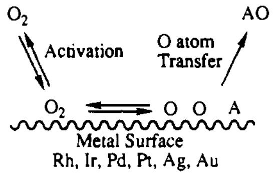

### Scheme II

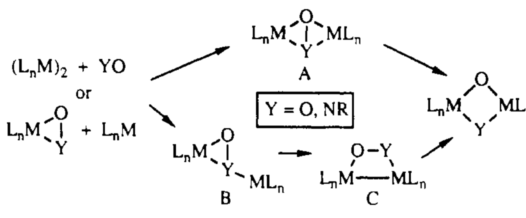

## Results

**Synthesis of [Cp*Rh($\mu$-Cl)]$_2$ (1).** Addition of excess Na(Hg) (0.4%) to an orange-red solution of [Cp*Rh($\mu$-Cl)Cl]$_2$ (Cp* = $C_5Me_5$ = pentamethylcyclopentadienyl) in methylene chloride rapidly gives a dark brown and then, after several hours, a dark blue solution.[6] The blue-black product [Cp*Rh($\mu$-Cl)]$_2$ (**1**) is isolated (65–75% yield) by crystallization from $CH_2Cl_2$/hexane at –40 °C (eq 1). The reaction must not be run longer than a few hours since **1** reacts slowly (12 h) with $CH_2Cl_2$ to regenerate

---

(1) Madix, R. J. In *Oxygen Complexes and Oxygen Activation by Transition Metals*; Martell, A. E., Sawyer, D. T., Eds.; Plenum Press: New York, 1988; p 253.

(2) A few late-transition-metal systems may achieve this but are complicated by following reactions of the proposed oxo complexes. See: (a) Egan, J. W.; Haggerty, B. S.; Rheingold, A. L.; Sendlinger, S. C.; Theopold, K. H. *J. Am. Chem. Soc.* **1990**, *112*, 2445. (b) Day, V. W.; Klemperer, W. G.; Lockledge, S. P.; Main, D. J. *J. Am. Chem. Soc.* **1990**, *112*, 2031. (c) Cotton, F. A.; Lahuerta, P.; Sanau, M.; Schwotzer, W. *Inorg. Chim. Acta* **1986**, *120*, 153.

(3) (a) Morse, D. B.; Rauchfuss, T. B.; Wilson, S. R. *J. Am. Chem. Soc.* **1988**, *110*, 8234. (b) Parkin, G.; Bercaw, J. E. *Polyhedron* **1988**, *7*, 2053. (c) Groves, J. T.; Ahn, K.-H. *Inorg. Chem.* **1987**, *26*, 3831. (d) Herrmann, W. A.; Serrano, R.; Bock, H. *Angew. Chem., Int. Ed. Engl.* **1984**, *23*, 383. (e) Chisholm, M. H.; Folting, K.; Huffman, J. C.; Kirkpatrick, C. C. *Inorg. Chem.* **1984**, *23*, 1021–1037. (f) Lever, A. P. B.; Wilshire, J. P.; Whan, S. K. *Inorg. Chem.* **1981**, *20*, 761. (g) Ledon, H. J.; Bonnet, M.; Galland, D. *J. Am. Chem. Soc.* **1981**, *103*, 6209. (f) Chin, D. H.; LaMar, G. N.; Balch, A. L. *J. Am. Chem. Soc.* **1980**, *102*, 5947. (g) Lemenovskii, D. A.; Baukova, T. V.; Fedin, V. P. *J. Organomet. Chem.* **1977**, *132*, C14.

(4) Leading reference: Ge, Y.-W.; Sharp, P. R. *Inorg. Chem.* **1992**, *31*, 379–384.

(5) Portions of this work have appeared as a communication: Sharp, P. R.; Hoard, D.; Barnes, C. L. *J. Am. Chem. Soc.* **1990**, *112*, 2024–2026.

(6) This synthesis is very similar to a synthesis used to prepare the phosphide analog of **1**, [Cp*Rh($\mu$-PMe$_2$)]$_2$, where [Cp*Rh($\mu$-PMe$_2$)Cl]$_2$ is reduced with Na/Hg: Werner, H.; Klingert, B.; Rheingold, A. L. *Organometallics* **1988**, *7*, 911–917.

0020-1669/93/1332-0612$04.00/0

**Table I.** Crystallographic and Data Collection Parameters

| | 1 | $4\cdot CH_2Cl_2$ | 5 | $6\cdot 0.5CH_2Cl_2$ |
|---|---|---|---|---|
| formula | $Rh_2C_{20}H_{30}Cl_2$ | $RhC_{19}H_{41}ClP_3\cdot CH_2Cl_2$ | $Rh_2C_{26}H_{35}Cl_2NO$ | $Rh_2C_{26}H_{35}BClF_4NO\cdot 0.5CH_2Cl_2$ |
| fw | 547.18 | 585.74 | 654.29 | 755.11 |
| space group | $C2/c$ (No. 15) | $C2/c$ (No. 15) | $P\bar{1}$ (No. 2) | $P2_1/c$ (No. 14) |
| $T$, °C | 22 | −100 | 22 | −100 |
| λ, Å | 0.71069 | 0.71069 | 0.71069 | 0.71069 |
| $a$, Å | 33.068(8) | 16.618(5) | 9.290(3) | 10.933(4) |
| $b$, Å | 13.173(3) | 12.074(6) | 17.830(3) | 15.166(6) |
| $c$, Å | 16.810(4) | 27.319(7) | 8.941(3) | 18.136(10) |
| $\alpha$, deg | | | 92.60(2) | |
| $\beta$, deg | 117.77(2) | 99.04(2) | 110.87(3) | 95.33(4) |
| $\gamma$, deg | | | 104.36(2) | |
| $V$, Å$^3$ | 6479.4 | 5413(3) | 1325.9 | 2994.2(2) |
| $Z$ | 12 | 8 | 2 | 4 |
| $d_{calc}$, g cm$^{-3}$ | 1.68 | 1.44 | 1.64 | 1.68 |
| $\mu(MoK_\alpha)$, cm$^{-1}$ | 17.6 | 11.0 | 14.5 | 13.1 |
| transm range, % | 90.3–99.7 | | 68.0–100 | 90.3–100 |
| $R(F_o)$[a] | 0.040 | 0.037 | 0.045 | 0.030 |
| $R_w(F_o)$[b] | 0.047 | 0.058 | 0.057 | 0.043 |

[a] $R(F_o) = \Sigma||F_o| - |F_c||/\Sigma|F_o|$. [b] $R_w(F_o) = [\Sigma w(|F_o| - |F_c|)^2/\Sigma wF_o^2]^{1/2}$.

**Table II.** Positional Parameters for 1

| atom | $x$ | $y$ | $z$ | $B$,[a] Å$^2$ |
|---|---|---|---|---|
| Rh1 | 0.21330(2) | 0.42995(7) | 0.63295(5) | 3.10(2) |
| Rh2 | 0.12719(2) | 0.42877(7) | 0.59615(5) | 3.53(2) |
| Rh3 | 0.04230(2) | 0.07367(7) | −0.23752(5) | 3.44(2) |
| Cl1 | 0.18772(9) | 0.3708(3) | 0.7377(2) | 5.05(8) |
| Cl2 | 0.15862(9) | 0.3104(3) | 0.5310(2) | 5.76(8) |
| Cl3 | −0.0186(1) | 0.1623(3) | −0.3580(2) | 9.8(1) |
| C1 | 0.2800(3) | 0.419(1) | 0.6338(6) | 4.7(3) |
| C2 | 0.2860(3) | 0.4555(8) | 0.7160(7) | 4.0(3) |
| C3 | 0.2613(3) | 0.5484(8) | 0.7028(6) | 4.1(3) |
| C4 | 0.2402(3) | 0.572(1) | 0.6097(7) | 4.7(3) |
| C5 | 0.2492(3) | 0.491(1) | 0.5640(6) | 5.2(3) |
| C6 | 0.3009(4) | 0.324(1) | 0.6191(9) | 8.9(4) |
| C7 | 0.3139(5) | 0.406(1) | 0.8086(9) | 9.7(5) |
| C8 | 0.2605(4) | 0.613(1) | 0.7776(8) | 8.3(4) |
| C9 | 0.2183(4) | 0.670(1) | 0.567(1) | 9.9(5) |
| C10 | 0.2338(5) | 0.475(2) | 0.4659(8) | 11.0(6) |
| C11 | 0.0512(3) | 0.419(1) | 0.5306(7) | 4.8(3) |
| C12 | 0.0665(3) | 0.4495(9) | 0.6162(7) | 5.0(3) |
| C13 | 0.0921(4) | 0.5394(9) | 0.6331(8) | 5.7(3) |
| C14 | 0.0913(3) | 0.573(1) | 0.5531(8) | 6.7(3) |
| C15 | 0.0679(3) | 0.491(1) | 0.4839(7) | 6.8(4) |
| C16 | 0.0225(5) | 0.325(1) | 0.487(1) | 8.3(5) |
| C17 | 0.0600(4) | 0.394(1) | 0.6911(8) | 9.7(5) |
| C18 | 0.1139(5) | 0.598(1) | 0.724(1) | 11.6(6) |
| C19 | 0.1068(5) | 0.672(1) | 0.533(1) | 14.2(7) |
| C20 | 0.0591(5) | 0.481(2) | 0.3905(8) | 14.4(7) |
| C21 | 0.0964(3) | 0.0577(9) | −0.2776(6) | 4.4(3) |
| C22 | 0.1167(3) | 0.0789(9) | −0.1879(6) | 3.7(2) |
| C23 | 0.1041(3) | 0.0006(9) | −0.1434(6) | 4.0(3) |
| C24 | 0.0773(3) | −0.0718(9) | −0.2086(6) | 4.2(3) |
| C25 | 0.0700(3) | −0.0351(9) | −0.2939(6) | 4.3(3) |
| C26 | 0.0997(5) | 0.123(1) | −0.3505(7) | 8.2(4) |
| C27 | 0.1477(4) | 0.169(1) | −0.142(1) | 7.8(4) |
| C28 | 0.1184(5) | −0.007(1) | −0.0436(8) | 8.3(5) |
| C29 | 0.0618(4) | −0.176(1) | −0.192(1) | 8.3(4) |
| C30 | 0.0442(5) | −0.087(1) | −0.3849(8) | 8.6(5) |

[a] Thermal parameters are given in the form of the isotropic equivalent displacement parameter defined as $(4/3)[a^2\beta(1,1) + b^2\beta(2,2) + c^2\beta(3,3) + ab(\cos\gamma)\beta(1,2) + ac(\cos\beta)\beta(1,3) + bc(\cos\alpha)\beta(2,3)]$.

the starting material, $[Cp^*Rh(\mu\text{-}Cl)Cl]_2$. Other solvents (THF and toluene) give poor yields and impure product, probably due to overreduction[7] resulting from the poor solubility of the starting material in these solvents. $Cp_2Co$ was also used as the reducing agent but gave variable yields. The nature of the problem associated with the use of cobaltacene was not pursued.

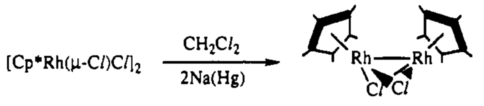

(1)

1

The $^1H$ NMR spectra of 1 are simple, showing a sharp singlet at 1.59 ppm in $C_6D_6$ and at 1.73 ppm in $CD_2Cl_2$. These shifts are slightly downfield from the precursor, opposite to what might be expected for a more electron-rich complex. Since the NMR data give no indication as to the possible nuclearity of 1, an X-ray crystal structure determination was undertaken.

A summary of crystallographic and data collection parameters is given in Table I. Crystallographic coordinates are given in Table II. Selected interatomic distances and angles are given in Table III. The unit cell contains two independent molecules, one in a general position (molecule A) and the other on a crystallographic 2-fold axis (molecule B). An ORTEP drawing of molecule A is shown in Figure 1. An ORTEP drawing of molecule B is included in the supplementary material. Both molecules contain two bonded Cp* capped Rh centers bridged by two chlorides. The primary difference between the two molecules is the mutual orientation of the two Cp* rings. In molecule A the Cp* rings are eclipsed while in molecule B they are staggered (illustrative drawing supplied as supplementary material). While staggering reduces the smallest inter-ring Me–Me contacts from 3.45 Å in A to 3.65 Å in B, the Rh–Rh distance is actually longer in B (2.628 Å) than in A (2.617 Å). What does shorten in B is the Rh–Cl distance (2.392 and 2.393 Å) versus that in A (2.411 and 2.408). Both molecules appear to show a trans influence of the Rh–Rh bond on the Rh–Cp* carbon distances. Those approximately "trans" to the Rh–Rh bond (C1 and C11 in A and C21 and C22 in B) are at the long end (all at 2.20 Å) of the range of Rh–C distances (2.20 to 2.13 Å).

The core of 1 is folded to give a "butterfly" geometry. Rh complexes with similar folded butterfly core geometries are $[(Cp^*Rh)_2(\mu\text{-}PPh_2)(\mu\text{-}PMe_2)]$, $[CpRh(\mu\text{-}SPh)]_2$, $[Cp^*Rh(\mu\text{-}CO)_2^{2-}$, and $[CpRh(\mu\text{-}pz)]_2$.[6,8] In this group, the Rh–Rh distances range from 2.795 to 2.611 Å, placing 1 at the low end of the range. Most similar are the P- and S-bridged complexes. A comparison of distances and angles for these complexes with those of 1 is included in Table IV. Apparent is the decrease in the Rh–Rh distance as the Rh–X distance increases. This is accompanied by decreases in the Rh–X–Rh angles and the "bend"

---

[7] The product of full reduction is currently under investigation.

[8] (a) Connelly, N. G.; Johnson, G. A.; Kelly, B. A.; Woodward, P. *J. Chem. Soc., Chem. Commun.* **1977**, 436. (b) Krause, M. J.; Bergman, R. G. *J. Am. Chem. Soc.* **1985**, *107*, 2972. (c) Bailey, J. A.; Grundy, S. L.; Stobart, S. R. *Organometallics* **1990**, *9*, 536.

**Table III.** Selected Intramolecular Distances (Å) and Angles (deg) for **1**

| | | | |
|---|---|---|---|
| | Molecule A | | |
| Rh1–Rh2 | 2.617(1) | Rh2–Cl2 | 2.402(4) |
| Rh1–Cl1 | 2.411(4) | Rh2–C11 | 2.227(9) |
| Rh1–Cl2 | 2.408(3) | Rh2–C12 | 2.20(1) |
| Rh1–C1 | 2.20(1) | Rh2–C13 | 2.13(1) |
| Rh1–C2 | 2.171(9) | Rh2–C14 | 2.18(1) |
| Rh1–C3 | 2.144(9) | Rh2–C15 | 2.15(1) |
| Rh1–C4 | 2.18(1) | Cl1–Cl2 | 3.244(4) |
| Rh1–C5 | 2.16(1) | Cp1–Rh1 | 1.800 |
| Rh2–Cl1 | 2.411(2) | Cp2–Rh2 | 1.806 |
| Rh2–Rh1–Cl1 | 57.13(6) | Rh1–Rh2–Cl2 | 57.14(7) |
| Rh2–Rh1–Cl2 | 56.94(9) | Cl1–Rh2–Cl2 | 84.7(1) |
| Cl1–Rh1–Cl2 | 84.6(1) | Rh1–Rh2–Cp2 | 150.5 |
| Rh2–Rh1–Cp1 | 150.4 | Cl1–Rh2–Cp2 | 134.1 |
| Cl1–Rh1–Cp1 | 133.7 | Cl2–Rh2–Cp2 | 137.8 |
| Cl2–Rh1–Cp1 | 138.5 | Rh1–Cl1–Rh2 | 65.74(8) |
| Rh1–Rh2–Cl1 | 57.13(9) | Rh1–Cl2–Rh2 | 65.92(9) |
| | Molecule B | | |
| Rh3–Rh3′ | 2.628(1) | Rh3–C23 | 2.143(9) |
| Rh3–Cl3 | 2.392(3) | Rh3–C24 | 2.17(1) |
| Rh3–Cl3′ | 2.393(5) | Rh3–C25 | 2.14(1) |
| Rh3–C21 | 2.20(1) | Cl3–Cl3′ | 3.246(6) |
| Rh3–C22 | 2.200(8) | Rh3–Cp3 | 1.805 |
| Rh3′–Rh3–Cl3 | 56.7(1) | Cl3–Rh3–Cp3 | 136.1 |
| Rh3′–Rh3–Cl3′ | 56.67(7) | Cl3′–Rh3–Cp3 | 135.8 |
| Cl3–Rh3–Cl3′ | 85.4(1) | Rh3–Cl3–Rh3′ | 66.6(1) |
| Rh3′–Rh3–Cp3 | 150.5 | | |

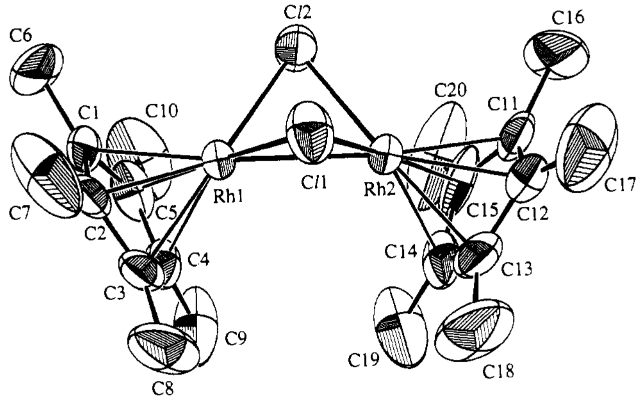

**Figure 1.** ORTEP drawing of the general position molecule (molecule A) of **1**, with 50% probability ellipsoids.

**Table IV.** Structural Comparison of $[(C_5R_5)Rh(\mu\text{-}X)]_2$ Complexes[a]

| complex | Rh–Rh | Rh–X | Rh–X–Rh | flap[e] | bend[f] |
|---|---|---|---|---|---|
| $[Cp^*Rh(\mu\text{-}Cl)]_2$[b] | 2.623 av | 2.401 av | 66.1 av | 107.6 | 95.7 av |
| $[CpRh(\mu\text{-}SPh)]_2$[c] | 2.644 | 2.306 av | 70.0 av | 106.5 | 98.5 |
| $[Cp^*Rh]_2(\mu\text{-}PMe_2)(PPh_2)$[d] | 2.795 | 2.235 av | 77.6 av | 111.5 | 110.0 |

[a] Distances are given in Å and angles are given in deg (av = average). [b] This work. [c] Reference 8a. [d] Reference 6. [e] Dihedral angle of Rh–X–Rh planes. [f] Dihedral Angle of X–Rh–X planes.

angle (dihedral angle between the X–Rh–X planes). The "flap" angle (dihedral angle between the Rh–X–Rh planes) does not seem to be correlated with these other parameters. Although the Rh–Rh distance in **1** is short, facile insertions into the Rh–Rh bond are observed.

**$[(Cp^*Rh)_2(\mu\text{-}Cl)(Cl)(\mu,\eta^1{:}\eta^2\text{-}O_2)]$ (2).** The injection of 1 equiv of $O_2$ into a $CH_2Cl_2$ solution of **1** at ca −60 °C rapidly produces a red solution. Variable-temperature $^1H$ NMR spectroscopy shows the presence of a single new fluxional product, **2**, to which we assign the structure shown in eq 2 based on the NMR data, reactivity, and the structure of the PhNO analogue (see below). At −70 °C two closely spaced Cp* resonances are observed. As the temperature is increased, the two resonances collapse and coalesce and grow into a single resonance at a chemical shift midway between the two low temperature peaks (see eq 2, $\Delta G^\ddagger \sim 50$ kJ/mol). The process is reversible provided that the temperature is kept below ca −15 °C. Above this temperature slow decomposition of the complex is evidenced by a darkening of the solution and the growth of several new Cp* peaks in the $^1H$ NMR spectra. Solid samples are much more stable and are obtained by solvent removal in vacuo at low temperatures. IR spectroscopy (mineral oil mull) shows the presence of the $O_2$ ligand as the only new band at 812 cm$^{-1}$. The expected isotopic shift to 768 cm$^{-1}$ is observed with $^{18}O_2$ substitution.

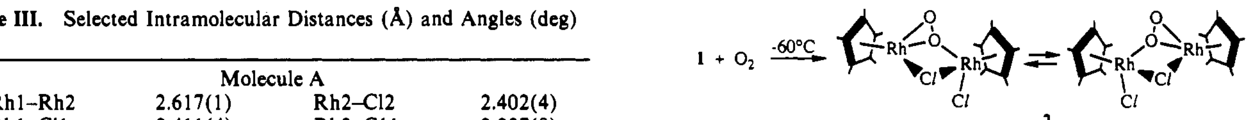

**2** (2)

**Reactions of 2 with Phosphines.** The addition of 2 equiv of $PPh_3$ to a cold solution of **2** rapidly forms a green and then a red solution. $^1H$ and $^{31}P$ NMR spectra indicate the formation of two products. One of these is readily identified as the known complex $Cp^*RhCl_2(PPh_3)$.[9] The other product, unstable above ca. 0 °C, has very similar spectroscopic properties and is believed to be $Cp^*Rh(O_2)(PPh_3)$ (**3**) (eq 3). Similar reactions were attempted with other phosphines ($PMePh_2$, $PMe_2Ph$, $PMe_3$) in the hope of producing a more stable analog of **3** or an oxo complex by oxygen atom abstraction. However, with the exception of $PMe_3$, these other phosphines produced complex mixtures (by $^{31}P$ NMR spectroscopy), and no attempts were made to isolate the products. For $PMe_3$, a larger phosphine-to-**2** ratio is required to completely consume **2** and to obtain a major product.

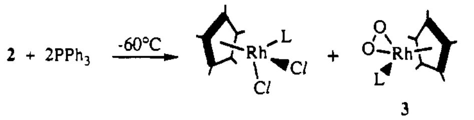

**3** (3)

The addition of 6 equiv of $PMe_3$ to a solution of **2** in methylene chloride at −78 °C gives a rapid color change from red to brown. IR spectroscopy of the reaction mixture shows an OH absorption, suggesting the presence of either $H_2O_2$ or $H_2O$. $^1H$ NMR spectra show a peak in the region for dissolved water which increases in intensity with the addition of water. $^{31}P$ NMR and $^1H$ NMR spectroscopy show the formation of a single major Rh containing product identified as the fulvene complex, $[(\eta^4\text{-}C_5Me_4CH_2)Rh(PMe_3)_3]Cl$ (**4**) (eq 4). The low-temperature $^{31}P$ NMR spectra indicate two magnetically equivalent $PMe_3$ ligands coupled to a third $PMe_3$ ligand. As the temperature is increased all three phosphine ligands become equivalent. The $^{13}C$ NMR spectrum of **4** was obtained at +25 and −50 °C. The two spectra show that the $PMe_3$ ligands give the only temperature dependent signals. The 25 °C spectrum shows a triplet and a doublet for the four Me groups of the fulvene ligand and a broad resonance corresponding to the Me groups of the $PMe_3$ ligands. At −50 °C the fulvene ligand signals are unchanged while the broad $PMe_3$ resonance is replaced with a triplet, corresponding to the two equivalent $PMe_3$ ligands, and a doublet, corresponding to the

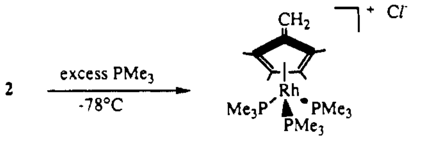

**4** (4)

---

[9] Kang, J. W.; Moseley, K.; Maitlis, P. M. *J. Am. Chem. Soc.* **1969**, *91*, 5970–5977.

**Table V.** Selected Positional Parameters for **4**

| | *x* | *y* | *z* | $B_{iso}$,[a] Å$^2$ |
|---|---|---|---|---|
| Rh1 | 0.194650(20) | 0.04274(3) | 0.140486(13) | 1.186(18) |
| P1 | 0.20677(7) | −0.00611(11) | 0.05971(5) | 1.57(5) |
| P2 | 0.23443(8) | 0.22358(10) | 0.12893(5) | 1.75(5) |
| P3 | 0.05270(7) | 0.07868(11) | 0.12693(5) | 1.62(5) |
| C1 | 0.1589(3) | −0.0704(4) | 0.21559(19) | 1.91(19) |
| C2 | 0.2099(3) | 0.0281(4) | 0.22357(18) | 1.77(20) |
| C3 | 0.2852(3) | 0.0048(4) | 0.20615(18) | 1.79(20) |
| C4 | 0.2733(3) | −0.0908(4) | 0.17557(17) | 1.55(18) |
| C5 | 0.1901(3) | −0.1262(4) | 0.17417(18) | 1.64(19) |
| C6 | 0.0979(3) | −0.1031(5) | 0.23891(22) | 2.38(23) |
| C7 | 0.2004(4) | 0.1128(5) | 0.26239(21) | 2.48(24) |
| C8 | 0.3658(3) | 0.0565(5) | 0.22419(23) | 2.9(3) |
| C9 | 0.3409(3) | −0.1535(5) | 0.15708(22) | 2.04(23) |
| C10 | 0.1547(3) | −0.2334(4) | 0.15291(21) | 1.95(22) |
| C11 | −0.0083(4) | −0.0428(5) | 0.11157(25) | 2.5(3) |
| C12 | 0.0037(3) | 0.1775(5) | 0.08122(23) | 2.31(24) |
| C13 | 0.0081(3) | 0.1282(5) | 0.17944(22) | 2.48(24) |
| C14 | 0.2012(4) | 0.3231(5) | 0.17154(24) | 2.8(3) |
| C15 | 0.3425(4) | 0.2545(6) | 0.1359(3) | 3.0(3) |
| C16 | 0.2009(4) | 0.2918(5) | 0.06963(23) | 2.76(25) |
| C17 | 0.3043(3) | 0.0213(6) | 0.03972(23) | 2.65(25) |
| C18 | 0.1353(3) | 0.0496(5) | 0.00841(21) | 2.25(24) |
| C19 | 0.1940(4) | −0.1516(5) | 0.04395(22) | 2.45(25) |

[a] $B_{iso}$ is the mean of the principal axes of the thermal ellipsoid.

**Table VI.** Selected Intramolecular Distances (Å) and Angles (deg) for **4**

| | | | |
|---|---|---|---|
| Rh1–P1 | 2.3233(14) | C1–C6 | 1.339(7) |
| Rh1–P2 | 2.3173(16) | C2–C3 | 1.435(7) |
| Rh1–P3 | 2.3697(14) | C2–C7 | 1.500(7) |
| Rh1–C2 | 2.251(5) | C3–C4 | 1.420(7) |
| Rh1–C3 | 2.201(5) | C3–C8 | 1.488(8) |
| Rh1–C4 | 2.198(5) | C4–C5 | 1.441(7) |
| Rh1–C5 | 2.244(5) | C4–C9 | 1.507(7) |
| C1–C2 | 1.457(7) | C5–C10 | 1.501(7) |
| C1–C5 | 1.479(7) | | |
| | | | |
| P1–Rh1–P2 | 92.33(5) | C2–C3–C4 | 107.8(4) |
| P1–Rh1–P3 | 97.52(5) | C2–C3–C8 | 126.4(5) |
| P2–Rh1–P3 | 95.99(5) | C4–C3–C8 | 124.8(5) |
| C2–C1–C5 | 102.7(4) | C3–C4–C5 | 107.6(4) |
| C2–C1–C6 | 129.5(5) | C3–C4–C9 | 124.2(4) |
| C5–C1–C6 | 127.7(5) | C5–C4–C9 | 127.2(5) |
| C1–C2–C3 | 108.0(4) | C1–C5–C4 | 107.1(4) |
| C1–C2–C7 | 122.6(5) | C1–C5–C10 | 121.7(4) |
| C3–C2–C7 | 124.2(5) | C4–C5–C10 | 125.6(4) |

third PMe$_3$ ligand. The closely related complex [Co($\eta^4$-C$_4$H$_6$)(PMe$_3$)$_3$]BPh$_4$ has very similar NMR properties.[10] Further analysis of the $^{13}$C NMR spectrum reveals three resonances corresponding to the five internal carbons of the fulvene ring along with a resonance for the exocyclic methylene group. Interestingly, $^{13}$C–$^{103}$Rh coupling is observed for the exocyclic methylene carbon as well as for the two sets of internal carbons of the fulvene. The presence of coupling to the exocyclic methylene carbon is unexpected based on the long distance between the Rh and the exocyclic methylene carbon as shown by the X-ray crystal structure determination.

A summary of crystallographic and data collection parameters is given in Table I. Crystallographic coordinates are given in Table V. Selected interatomic distances and angles are given in Table VI. An ORTEP drawing of **4** is shown in Figure 2. The cationic portion is a classical three-legged piano stool structure where the fulvene "seat" interacts with the Rh through only four carbons of the ring as in a butadiene complex. The exocyclic C–C double bond is not coordinated and is folded up away from the Rh center, forming an angle of 24.8(3)° with the coordinated portion of the ring. As such, the structure is closely related to a number of complexes of general formula [(1,4-diene)ML$_3$]$^{n+}$, including several fulvene complexes.[10,11]

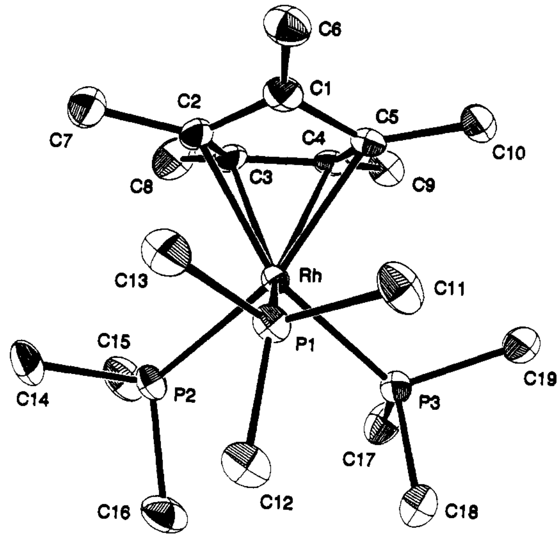

**Figure 2.** ORTEP drawing of the cationic portion of **4**, with 50% probability ellipsoids.

**[(Cp*Rh)$_2$($\mu$-Cl)(Cl)($\mu$,$\eta^1$:$\eta^2$-PhNO)] (5).** The addition of 1 equiv of nitrosobenzene to a toluene solution of **1** rapidly produces a dark red solution. After the solution is reduced, layered with hexane, and cooled to −40 °C, dark red crystals of **5** are isolated in a 75% yield (eq 5). IR spectroscopy reveals the NO absorption band at 986 cm$^{-1}$, suggesting a reduction in the NO bond order. The $^1$H NMR spectrum shows two resonances for the nonequivalent Cp* groups, as expected from the solid-state structure (see below). However, the phenyl region is more complex than expected for a freely rotating phenyl ring. Fast rotation of the nitrosobenzene phenyl ring about the ipso-C–N bond would give a total of three resonances for the ortho, meta, and para hydrogen atoms. With restricted rotation, all five hydrogen atoms are nonequivalent. Four signals are observed, two doublets corresponding to the two ortho hydrogen atoms, a triplet corresponding to the para hydrogen (presumably the coupling constants between the para hydrogen atom and the two meta hydrogen atoms are nearly identical), and a multiplet for the two meta hydrogen atoms. The $^{13}$C NMR spectrum shows six carbon atoms in the phenyl region supporting restricted rotation. A rotational barrier is consistent with the "sandwiching" of the phenyl ring between the Cp* groups as revealed by the X-ray crystal structure determination.

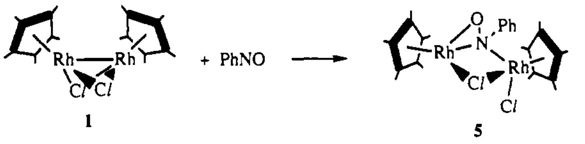

(5)

A summary of crystallographic and data collection parameters for **5** is given in Table I. Crystallographic coordinates are given in Table VII. Selected interatomic distances and angles are given in Table VIII. The structure is disordered and was modeled with two superimposed orientations of the molecule. The major orientation (65%) has O bonded to one Rh and a terminal Cl bonded to the other Rh. This is reversed in the minor orientation

---

(10) de Carvalho, L. C. A.; Peres, Y.; Dartiguenave, M.; Dartiguenave, Y.; Beauchamp, A. L. *Organometallics* **1985**, 2021–2029.

(11) (a) Glueck, D. S.; Bergman, R. G. *Organometallics* **1990**, *9*, 2862–2863. (b) Kreindlin, A. Z.; Fedin, E. I.; Petrovski, P. V.; Rybinskaya, M. I. *Organometallics* **1991**, *10*, 1206–1209. (c) Schäufele, H.; Hu, D.; Pritzkow, H.; Zenneck, U. *Organometallics* **1989**, *8*, 396–401. (d) de Carvalho, L. C. A.; Dartiguenave, M.; Dahan, F.; Dartiguenave, Y.; Dubac, J.; Laporterie, A.; Manuel, G.; Iloughmane, H. *Organometallics* **1986**, *5*, 2205–2211. (e) Chappel, S. D.; Cole-Hamilton, D. J.; Galas, A. M. R.; Hursthouse, M. B. *J. Chem. Soc., Dalton Trans.* **1982**, 1867–1871.

**Table VII.** Positional Parameters for **5**

| atom[a] | *x* | *y* | *z* | *B*,[b] Å$^2$ |
|---|---|---|---|---|
| Rh1 | 0.14717(4) | 0.31293(2) | 0.48969(4) | 3.641(9) |
| Rh2 | –0.10684(4) | 0.14061(2) | 0.27545(4) | 3.556(8) |
| Cl1 | 0.0557(2) | 0.18411(7) | 0.5650(2) | 5.01(3) |
| Cl2 | 0.1376(2) | 0.1322(1) | 0.2380(2) | 4.52(4) |
| Cl2′ | –0.1042(4) | 0.3444(2) | 0.4751(4) | 4.37(8) |
| O | –0.0917(5) | 0.2997(3) | 0.3930(6) | 4.4(1) |
| O′ | 0.097(1) | 0.1893(6) | 0.243(1) | 5.4(3) |
| N | –0.0420(6) | 0.2617(3) | 0.2834(7) | 3.5(1) |
| N′ | 0.029(1) | 0.2476(7) | 0.257(1) | 4.3(3) |
| C1 | 0.3996(6) | 0.3248(3) | 0.5938(7) | 4.9(1) |
| C2 | 0.3589(6) | 0.3630(3) | 0.7095(7) | 4.8(1) |
| C3 | 0.2975(6) | 0.4238(3) | 0.6447(7) | 4.9(1) |
| C4 | 0.2956(7) | 0.4229(3) | 0.4810(8) | 5.7(2) |
| C5 | 0.3675(6) | 0.3618(4) | 0.4547(7) | 5.5(1) |
| C6 | 0.4695(7) | 0.2571(4) | 0.6188(9) | 7.8(2) |
| C7 | 0.3818(9) | 0.3438(5) | 0.8735(8) | 7.4(2) |
| C8 | 0.2413(8) | 0.4795(4) | 0.723(1) | 8.0(2) |
| C9 | 0.248(1) | 0.4796(4) | 0.369(1) | 9.8(2) |
| C10 | 0.3992(8) | 0.3423(6) | 0.3082(8) | 8.9(2) |
| C11 | –0.2670(6) | 0.0334(3) | 0.3000(7) | 4.7(1) |
| C12 | –0.2368(6) | 0.0196(3) | 0.1601(7) | 4.8(1) |
| C13 | –0.2863(7) | 0.0745(4) | 0.0576(7) | 5.8(2) |
| C14 | –0.3548(6) | 0.1211(3) | 0.1327(8) | 5.9(2) |
| C15 | –0.3386(6) | 0.0982(3) | 0.2847(7) | 5.2(1) |
| C16 | –0.2331(7) | –0.0093(4) | 0.4425(8) | 6.5(2) |
| C17 | –0.1595(8) | –0.0407(4) | 0.1296(9) | 6.9(2) |
| C18 | –0.284(1) | 0.0767(5) | –0.1089(8) | 8.4(2) |
| C19 | –0.4285(8) | 0.1849(4) | 0.065(1) | 10.1(3) |
| C20 | –0.3884(7) | 0.1309(4) | 0.4103(9) | 8.1(2) |
| C21 | –0.0486(8) | 0.2960(4) | 0.1324(7) | 6.9(2) |
| C22 | –0.0106(8) | 0.2656(4) | 0.0121(9) | 7.5(2) |
| C23 | –0.0386(8) | 0.3003(4) | –0.1313(9) | 7.2(2) |
| C24 | –0.1007(8) | 0.3627(4) | –0.1439(9) | 7.4(2) |
| C25 | –0.1405(8) | 0.3896(4) | –0.0268(8) | 7.1(2) |
| C26 | –0.1135(9) | 0.3566(4) | 0.1120(8) | 7.3(2) |

[a] Primed atoms represent the minor orientation. [b] Thermal parameters are given in the form of the isotropic equivalent displacement parameter defined as $(4/3)[a^2\beta(1,1) + b^2\beta(2,2) + c^2\beta(3,3) + ab(\cos\gamma)\beta(1,2) + ac(\cos\beta)\beta(1,3) + bc(\cos\alpha)\beta(2,3)]$.

**Table VIII.** Selected Intramolecular Distances (Å) and Angles (deg) for **5**

| | | | |
|---|---|---|---|
| Rh1–Cl1 | 2.456(1) | Rh2–O′ | 2.01(1) |
| Rh1–Cl2′ | 2.494(4) | Rh2–N | 2.083(6) |
| Rh1–O | 2.021(5) | Rh2–N′ | 2.06(1) |
| Rh1–N | 2.016(4) | Rh2–C11 | 2.185(5) |
| Rh1–N′ | 2.10(1) | Rh2–C12 | 2.189(5) |
| Rh1–C1 | 2.143(5) | Rh2–C13 | 2.113(5) |
| Rh1–C2 | 2.178(4) | Rh2–C14 | 2.127(5) |
| Rh1–C3 | 2.187(5) | Rh2–C15 | 2.131(6) |
| Rh1–C4 | 2.122(6) | O–N | 1.432(9) |
| Rh1–C5 | 2.155(6) | O′–N′ | 1.37(2) |
| Rh2–Cl1 | 2.457(1) | N–C21 | 1.495(9) |
| Rh2–Cl2 | 2.449(2) | N′–C21 | 1.53(1) |

| | | | |
|---|---|---|---|
| Cl1–Rh1–Cl2′ | 91.06(9) | Rh2–O′–N′ | 72.3(7) |
| Cl1–Rh1–O | 81.7(2) | Rh1–N–Rh2 | 110.3(3) |
| Cl1–Rh1–N | 80.1(2) | Rh1–N–O | 69.4(3) |
| Cl1–Rh1–N′ | 81.2(3) | Rh1–N–C21 | 117.7(4) |
| Cl2′–Rh1–N′ | 90.8(3) | Rh2–N–O | 111.7(4) |
| O–Rh1–N | 41.6(3) | Rh2–N–C21 | 119.8(4) |
| Cl1–Rh2–O′ | 85.2(3) | O–N–C21 | 117.4(6) |
| Cl1–Rh2–N | 78.8(1) | Rh1–N′–Rh2 | 108.1(6) |
| Cl1–Rh2–N′ | 81.9(3) | Rh1–N′–O′ | 110.2(7) |
| Cl1–Rh2–Cl2 | 88.28(6) | Rh1–N′–C21 | 111.7(7) |
| Cl2–Rh2–N | 91.4(2) | Rh2–N′–O′ | 68.4(6) |
| O′–Rh2–N′ | 39.3(5) | Rh2–N′–C21 | 119.6(5) |
| Rh1–Cl1–Rh2 | 86.49(5) | O′–N′–C21 | 131(1) |
| Rh1–O–N | 69.0(2) | | |

(35%). The Cp* and Ph groups, and the Rh and bridging Cl atoms of the two orientations overlap. The disorder is well modeled as shown by the good agreement between the comparable bond distances of the two orientation. An ORTEP drawing of the major orientation is shown in Figure 3, and one of the minor orientation is included in the supplementary material. The $\mu,\eta^1$:$\eta^2$-bonding mode has been observed in only a few other PhNO structures.[12] As observed in these and other $\pi$-bonded RNO complexes, the N–O bond length in **5** is longer than that in free-PhNO and is close to that expected for a N–O single bond.[13]

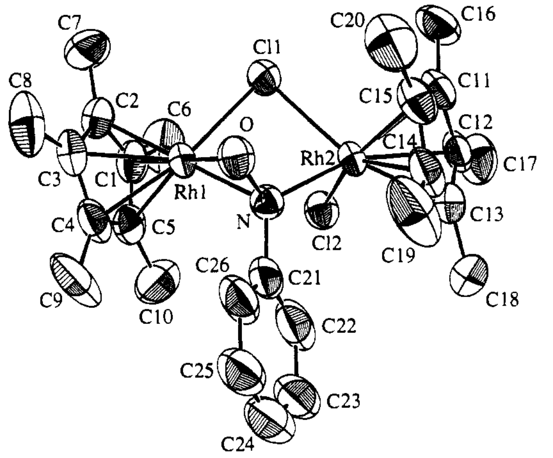

**Figure 3.** ORTEP drawing of the major orientation of **5**, with 50% probability ellipsoids.

Finally, the analogous 2-nitrosotoluene complex is prepared in a manner analogous to that of **4** but is not stable and decomposes rapidly in $CDCl_3$.

**$[(\mathrm{Cp}^*\mathrm{Rh})_2(\mu\text{-Cl})(\mu,\eta^2{:}\eta^2\text{-PhNO})]\mathrm{BF}_4$ (6).** The reaction of 1 equiv of $TlBF_4$ with **5** in THF immediately precipitates a red powder. Crystallization of the red product from $CH_2Cl_2$/ether at –40 °C gives red crystals of **6** in a 70% yield (eq 6). The $\nu_{NO}$ band is not observed in the IR spectra and may be buried under the B–F bands. The $^1$H NMR spectrum shows equivalent Cp* rings and a broad resonance and a triplet in the phenyl region. The $^{13}$C NMR spectrum shows three resonances in the phenyl region. As with **5**, it is probable that the nitrosobenzene phenyl ring suffers from hindered rotation. Finally, this complex is the least stable of the rhodium nitrosobenzene complexes described here. It decomposes slowly at room temperature under $N_2$ and quite quickly at ambient temperatures when exposed to air. However, it can be kept for long periods under $N_2$ at –40 °C. The $\mu,\eta^2$:$\eta^2$-bonding mode of the PhNO ligand expected in **6** is unique and was confirmed by an X-ray crystal structure determination.

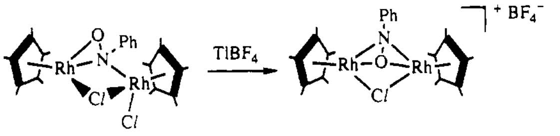

(6)

**5** **6**

A summary of crystallographic and data collection parameters is given in Table I. Crystallographic coordinates are given in Table IX. Selected interatomic distances and angles are given in Table X. An ORTEP drawing of the cationic portion is shown in Figure 4. The $\mu,\eta^2$:$\eta^2$ bonding mode is new in nitrosoarene coordination chemistry, and only recently has this bonding mode been found in dioxygen coordination chemistry.[14] The bonding to the Rh centers is very symmetrical, and though not crystallographically required, a mirror plane containing the PhNO ligand could easily divide the cation. The metrical parameters of the PhNO ligand are very similar to the $\eta^2$-portion of **5** indicating

---

(12) (a) Stella, S.; Floriani, C.; Chiesa-Villa, A.; Guastini, C. *J. Chem. Soc., Dalton Trans.* **1988**, 545. (b) Otsuka, S.; Aotani, Y.; Tatsuno, Y.; Yoshida, T. *Inorg. Chem.* **1976**, *15*, 656. Calligaris, M.; Yoshida, T.; Otsuka, S. *Inorg. Chim. Acta* **1974**, *11*, L15.

(13) Cameron, M.; Gowenlock, B. G. *Chem. Soc. Rev.* **1990**, *19*, 355–379.

(14) Kitajima, N.; Fujisawa, K.; Fujimoto, C.; Moro-oka, Y.; Hashimoto, S.; Kitagawa, T.; Toriumi, K.; Tatsumi, K.; Nakamura, A. *J. Am. Chem. Soc.* **1992**, *114*, 1277–1291.

**Table IX.** Selected Positional Parameters for **6**

| atom | *x* | *y* | *z* | $B,^a$ Å$^2$ |
|---|---|---|---|---|
| Rh1 | 0.91841(3) | 0.345647(21) | 0.881694(18) | 1.064(15) |
| Rh2 | 1.20019(3) | 0.326742(20) | 0.836203(18) | 1.098(14) |
| Cl | 1.11124(9) | 0.30947(7) | 0.95325(6) | 1.57(4) |
| O | 1.01538(24) | 0.30159(18) | 0.79317(15) | 1.34(11) |
| N | 1.0374(3) | 0.39240(21) | 0.80887(19) | 1.16(13) |
| C1 | 0.7902(4) | 0.2936(3) | 0.95397(24) | 1.49(17) |
| C2 | 0.7388(4) | 0.2846(3) | 0.87996(24) | 1.53(18) |
| C3 | 0.7315(4) | 0.3709(3) | 0.84549(24) | 1.42(17) |
| C4 | 0.7722(4) | 0.4344(3) | 0.90194(23) | 1.47(17) |
| C5 | 0.8119(4) | 0.3878(3) | 0.96837(23) | 1.41(17) |
| C6 | 0.8189(5) | 0.2215(3) | 1.0083(3) | 2.17(19) |
| C7 | 0.7026(4) | 0.2007(3) | 0.8413(3) | 2.00(20) |
| C8 | 0.6821(5) | 0.3917(4) | 0.7692(3) | 2.04(21) |
| C9 | 0.7740(4) | 0.5318(3) | 0.8914(3) | 1.86(19) |
| C10 | 0.8639(4) | 0.4253(3) | 1.0396(3) | 1.76(19) |
| C11 | 1.3801(4) | 0.2778(3) | 0.87188(23) | 1.45(18) |
| C12 | 1.3847(4) | 0.3716(3) | 0.8578(3) | 1.59(18) |
| C13 | 1.3451(4) | 0.3857(3) | 0.7820(3) | 1.72(18) |
| C14 | 1.3118(4) | 0.3019(3) | 0.74896(25) | 1.77(18) |
| C15 | 1.3365(3) | 0.2349(3) | 0.80520(24) | 1.54(17) |
| C16 | 1.4143(4) | 0.2347(3) | 0.9446(3) | 1.90(20) |
| C17 | 1.4304(5) | 0.4393(3) | 0.9128(3) | 2.18(22) |
| C18 | 1.3374(5) | 0.4731(3) | 0.7423(3) | 2.42(21) |
| C19 | 1.2657(5) | 0.2863(4) | 0.6704(3) | 2.42(21) |
| C20 | 1.3197(5) | 0.1384(3) | 0.7948(3) | 2.06(21) |
| C21 | 1.0110(4) | 0.4483(3) | 0.74645(23) | 1.33(16) |
| C22 | 0.9653(4) | 0.4173(3) | 0.6779(3) | 2.20(21) |
| C23 | 0.9447(5) | 0.4770(4) | 0.6203(3) | 2.90(24) |
| C24 | 0.9676(5) | 0.5654(3) | 0.6307(3) | 2.66(21) |
| C25 | 1.0125(5) | 0.5946(3) | 0.6983(3) | 2.36(22) |
| C26 | 1.0346(4) | 0.5375(3) | 0.7574(3) | 1.68(18) |

[a] Thermal parameters are the mean of the principal axes of the thermal ellipsoids.

**Table X.** Selected Intramolecular Distances (Å) and Angles (deg) for **6**

| | | | |
|---|---|---|---|
| Rh1–Cl | 2.4335(15) | Rh2–O | 2.132(3) |
| Rh1–O | 2.113(3) | Rh2–N | 2.060(3) |
| Rh1–N | 2.063(3) | Rh2–C11 | 2.145(4) |
| Rh1–C1 | 2.156(4) | Rh2–C12 | 2.130(4) |
| Rh1–C2 | 2.169(4) | Rh2–C13 | 2.136(4) |
| Rh1–C3 | 2.123(4) | Rh2–C14 | 2.120(4) |
| Rh1–C4 | 2.147(4) | Rh2–C15 | 2.152(4) |
| Rh1–C5 | 2.139(4) | O–N | 1.422(4) |
| Rh2–Cl | 2.4299(16) | N–C21 | 1.422(5) |
| ClRh1–O | 82.12(9) | Rh1–O–N | 68.23(17) |
| Cl–Rh1–N | 81.52(10) | Rh2–O–N | 67.46(17) |
| O–Rh1–N | 39.80(12) | Rh1–N–Rh2 | 105.13(15) |
| Cl–Rh2–O | 81.83(9) | Rh1–N–O | 71.97(17) |
| Cl–Rh2–N | 81.68(10) | Rh1–N–C21 | 128.4(3) |
| O–Rh2–N | 39.62(12) | Rh2–N–O | 72.91(17) |
| Rh1–Cl–Rh2 | 84.66(5) | Rh2–N–C21 | 125.9(3) |
| Rh1–O–Rh2 | 100.99(12) | O–N–C21 | 113.6(3) |

relatively little perturbation as a result of the $\eta^2$-bonding of the second Rh atom.

**$[Cp^*Rh(\mu,\eta^1:\eta^2\text{-}PhNO)]_2$ (7).** Complex **7** was first obtained as a product from the reaction of **5** with $PPh_3$ (see below). In seeking a better route to this complex we treated **5** with 2 equiv of Na(Hg) (0.4%), 1 equiv of $TlBF_4$, and excess nitrosobenzene (3 equiv) in THF. Initially, a small amount of red solid precipitates (probably complex **6**) which disappears after several hours. Dark red crystals of **7** are then isolated in a 70% yield from the reaction mixture by removing the volatiles in vacuo and recrystallizing the residue from toluene/hexane at –40 °C (eq 7).

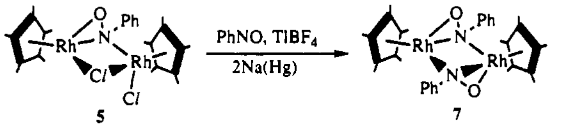

(7)

As with **5**, IR spectroscopy shows a low energy $\nu_{NO}$ band at 1001 cm$^{-1}$. The NMR spectra for **6** are also similar to those of **5**, revealing equivalent phenyl rings with hindered rotation. The $^1$H NMR spectrum of **7** includes one Cp* resonance and a complex phenyl region. The $^{13}$C NMR spectrum shows a phenyl region that is almost identical to the phenyl region of **5** with resonances for six carbons, again indicating hindered rotation. The CpCo analogue of **7** has been structurally characterized.[12a]

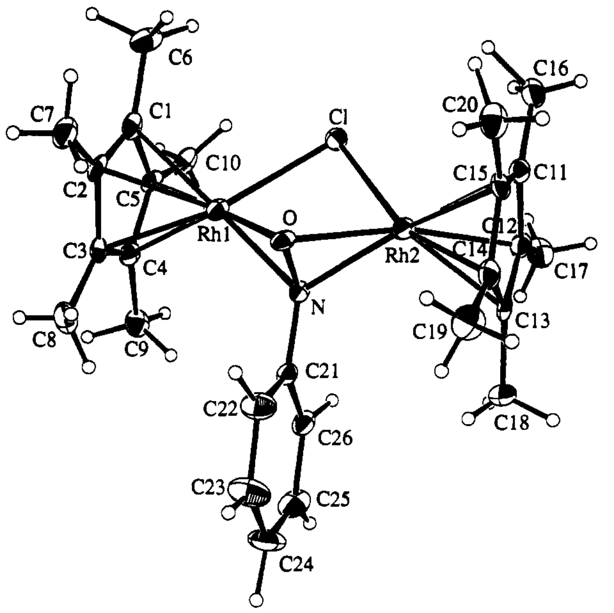

**Figure 4.** ORTEP drawing of the cationic portion of **6**, with 50% probability ellipsoids.

**Reactions of 5 with Phosphines.** $[(Cp^*Rh)_2(\mu\text{-}Cl)(Cl)(\mu,\eta^1:\eta^2\text{-}PhNO)]$ (**5**) was treated with L = $PPh_3$ and $PMe_3$ with the objective of producing an asymmetric cleavage of the molecule similar to the $PPh_3$ cleavage of the dioxygen complex **2** (eq 3). Such a reaction would yield two products, Cp*Rh(PhNO)L and $Cp^*RhCl_2L$ (or $[Cp^*RhClL_2]Cl$ with L = $PMe_3$). Unfortunately, the reactions of **5** with phosphines are not so simple. With 2 equiv of $PPh_3$ and **5** in toluene a slow reaction over the course of several days produces the dinitrosobenzene complex **7** as one of the major products (by $^1$H NMR spectroscopy). This complex presumably forms by the dimerization of monomeric rhodium nitrosobenzene fragments produced in the cleavage of **5**. $^{31}$P NMR spectroscopy reveals that $Cp^*RhCl_2(PPh_3)$[9] is also a reaction product, but not the major phosphine-containing complex. Small amounts of $Ph_3PO$ are also detected.

$PMe_3$ also give **6** as one of the major products. Since $PMe_3$ is much more nucleophilic than $PPh_3$, the reaction is much faster and is completed overnight. In this case, the $^{31}$P NMR spectrum of the reaction mixture in toluene (a precipitate, probably $[Cp^*RhCl(PMe_3)_2]Cl$, formed) includes a small resonance for $Me_3PO$ and a large unidentified broad resonance at –10 ppm.

**Reactions of CO with the Nitrosobenzene Complexes 5–7.** All three nitrosobenzene complexes were treated with CO (40 psi). Complex **5** gives, after 1.5–2 h, a color change from dark red to brilliant light red. IR spectroscopy reveals the formation of phenyl isocyanate, PhNCO (35%), which was confirmed by the addition of dry methanol and analysis of the resulting carbamate by HPLC. Trace amounts of phenyl urea, PhNHCONHPh, are also detected. The $^1$H NMR spectrum of the nonvolatile components of the reaction mixture includes four major Cp* resonances. Two of these peaks are identified as belonging to $[Cp^*Rh(\mu\text{-}Cl)Cl]_2$ and $Cp^*Rh(CO)_2$.[15] IR spectra shows CO bands from $Cp^*Rh(CO)_2$ along with other CO bands.

The reaction of CO with the nitrosobenzene salt **6** is more rapid and the solution's color changes from red to golden brown within 30 min. Analysis of the reaction mixture as above indicates

---

[15] Kang, J. W.; Maitlis, P. M. *J. Organomet. Chem.* **1971**, *26*, 393–399.

the formation of PhNCO (30%) and trace amounts of phenyl urea. Again, $^1$H NMR spectroscopy shows that $Cp^*Rh(CO)_2$ is produced along with other unknown $Cp^*Rh$ compounds. CO bands in the IR spectrum of the reaction mixture confirm the presence of $Cp^*Rh(CO)_2$ along with other CO-containing complexes.

Finally, there is no reaction between CO and the dinitrosobenzene complex **7** at 25 °C. At 40 °C a reaction does take place overnight with very little color change. By IR spectroscopy, PhNCO is not produced, and the only CO bands present correspond to $Cp^*Rh(CO)_2$. The $^1$H NMR spectrum confirms the clean formation of $Cp^*Rh(CO)_2$. HPLC analysis shows a trace of phenyl urea. The fate of the PhNO was not determined.

## Discussion

$[Cp^*Rh(\mu\text{-}Cl)]_2$ (**1**) is a member of an extensive family of Rh–Rh-bonded complexes of general formula $[(C_5R_5)Rh(\mu\text{-}X)]_2$ where $C_5R_5$ is Cp, Cp*, and indenyl and X is an anionic bridging ligand (e.g. halides, thiolates, phosphides, alkenyls).[6,8,16] In this family the reactivity of the Rh–Rh bond varies greatly. In the subfamily, X = SR, $R_2P$, and Cl, reactivity increases in the series. Thus, $[CpRh(SPh)]_2$ is air stable, $Cp^*Rh(PR_2)_2$ reacts with dioxygen but at the phosphide ligand[17] (insertions into the Rh–Rh bond of the phosphide complex do occur with Se and Te), and **1** is highly air sensitive and inserts dioxygen into the Rh–Rh bond. (A similar trend in reactivity is noted for the Co analogues.[18]) The reactivity trend is opposite to the Rh–Rh bond length trend (Table IV).

The reactivity of **1** can be described in terms of valence disproportionation of the Rh(II) centers. With dioxygen and nitrosobenzene, the products can be viewed either as dimers of Rh(I) and Rh(III) (dioxygen and nitrosobenzene as neutral ligands) or as dimers of Rh(III) (dioxygen and nitrosobenzene as dianionic ligands). The insertions of dioxygen and nitrosobenzene into the Rh–Rh bond of **1** are rare examples of such processes. Although binuclear complexes of these ligands have previously been prepared,[12,13,19] their synthesis by direct insertion into a M–M bond is uncommon.[20] In addition, the $\mu,\eta^1{:}\eta^2$-bonding mode is unusual having been found in only one other case for dioxygen[21] and in only a few cases for nitrosobenzene.[13] The extensive interaction of the $O_2$ and PhNO groups might be expected to reduce the bond order beyond that seen in nonbridging complexes. However, the IR and the X-ray data do not indicate any weakening or lengthening of the O–O or N–O bonds beyond that seen in other complexes. Thus, the $\nu_{NO}$ absorption of **5** (986 cm$^{-1}$) and **7** (1001 cm$^{-1}$) are close to those of nonbridging, side-on bonded nitrosobenzene metal complexes which are typically found at around 1000 cm$^{-1}$. In fact, the $\nu_{NO}$ band for the mononuclear complex, $Pt(PhNO)(PPh_3)_2$, is found at an even lower energy (973 cm$^{-1}$).[12b] Similarly, the $\nu_{OO}$ band for the dioxygen complex **2** (812 cm$^{-1}$) falls in the middle of the range for peroxo-type dioxygen complexes[22] and is very similar to that found for $[RhCl(PPh_3)_2(\mu,\eta^1{:}\eta^2\text{-}O_2)]_2$ (845 cm$^{-1}$), the only other complex with a $\mu,\eta^1{:}\eta^2$-dioxygen ligand.[21] The N–O bond lengths in **5** and **6** are also typical of structurally characterized $\eta^2$-PhNO complexes although the metrical parameters for **5** are in doubt due to the disorder.[23]

**Phosphine Reactions.** We had hoped that phosphines would abstract an oxygen atom from the dioxygen ligand of **2** to give an oxo complex. The observed rupture of the dimer is consistent with the chemistry of related complexes. The dioxygen (and the nitrosobenzene) complex can be viewed as an $[(L_2X)Rh(X)(\mu\text{-}X)]_2$ dimer (X = an anionic ligand, L = a neutral ligand) with the Cp* ligand equivalent to an $L_2X$ ligand set and the dioxygen ligand equivalent to an $(X)(\mu\text{-}X)$ ligand set. Such bridging systems are typically cleaved by added ligands.[24] Rupture must also occur for the PhNO complex with $PPh_3$; however, $PPh_3$ evidently coordinates only weakly to the $Cp^*Rh(PhNO)$ fragment, and loss of $PPh_3$ leads to dimerization to $[Cp^*Rh(PhNO)]_2$ (**7**).

With $PMe_3$, initial rupture of the dimer probably also occurs to form an analogue of **3**. The dioxygen may then be displaced by the $PMe_3$ ligand to give $Cp^*Rh(PMe_3)_2$. Displacement of dioxygen from late-transition-metal dioxygen complexes is known although, with phosphines, oxidation to phosphine oxide is usually observed.[25] $Cp^*Rh(PMe_3)_2$[26] is also a product of the $PMe_3$ reaction with the nitrosobenzene complex, suggesting displacement for PhNO as well.[27] The subsequent course of the reaction probably follows that observed in the oxidative deprotonation of Fe coordinated peralkylarene rings.[28] These reactions are believed to be initiated by electron transfer from the metal center to dioxygen followed by ring deprotonation by the resulting superoxide ion ultimately giving $H_2O_2$ and/or $H_2O$. Cp* ring deprotonations have recently been observed for Cp*Ir(III) complexes.[11a,29]

**CO Reactions.** The CO reactions of the nitrosobenzene complexes are of particular interest since these can function as models for the important carbonylation of nitroarenes to isocyanates.[30] Deoxygenation of the nitro group to give a nitrosoarene is a postulated first step in the process. Further carbonylations are believed to proceed either through an imido complex or through metallocyclic intermediates. Both of these pathways are considered in the reaction of our complexes.

Possible pathways for the reaction of **5** with CO are shown in Scheme III. As with other reactions involving **5**, it seems likely that the molecule is initially cleaved by CO giving stable $[Cp^*Rh(\mu\text{-}Cl)Cl]_2$ and a reactive nitrosobenzene–CO complex, which reacts with more CO to finally give PhNCO. Initial insertion of CO into the Rh–N nitrosobenzene bond is postulated based on the observed reactivity of this bond in other nitrosobenzene complexes.[19] Alternatively, initial insertion into the Rh–O bond with the subsequent loss of $CO_2$ would give the imido complex,

---

(16) (a) Dickson, R. S.; Fallon, G. D.; Nesbit, R. J.; Pain, G. N. *J. Organomet. Chem.* **1982**, *236*, C61. (b) Dickson, R. S.; Fallon, G. D.; Nesbit, R. J.; Pain, G. N. *Organometallics* **1985**, *4*, 355. (c) Baimbridge, C. W.; Dickson, R. S. Fallon, G. D.; Grayson, I.; Nesbit, R. J.; Weigold, J. *Aust. J. Chem.* **1986**, *39*, 1187. (d) Bieri, J. H.; Egolf, T.; von Philipsborn, W.; Piantini, U.; Prewo, R.; Ruppli, U.; Salzer, A. *Organometallics* **1986**, *5*, 2413. (e) Dickson, R. S.; Fallon, G. D.; Jenkins, S. M.; Skelton, B. W.; White, A. H. *J. Organomet. Chem.* **1986**, *314*, 333. (f) Dickson, R. S.; Gatehouse, B. M.; Johnson, S. H. *Acta Crystallogr., Sect. B* **1977**, *33*, 319. (g) Carl, R. T.; Hughes, R. P.; Rheingold, A. L.; Marder, T. B.; Taylor, N. J. *Organometallics* **1988**, *7*, 1613. (h) Caddy, P.; Green, M.; Smart, L. E.; White, N. *J. Chem. Soc., Chem. Commun.* **1978**, 839.

(17) Klingert, B.; Rheingold, A. L.; Werner, H. *Inorg. Chem.* **1988**, *27*, 1354–1358.

(18) Koelle, U.; Fuss, B.; Belting, M.; Raabe, E. *Organometallics* **1986**, *5*, 980–987.

(19) Gubelmann, M. H.; Williams, A. F. *Struct. Bonding* **1983**, *55*, 1–65.

(20) Binuclear dioxygen complexes by insertion of $O_2$ into Rh–Rh and Ir–Ir bonds: (a) Baranovskii, I. B.; Zhilyaeva, A. N.; Dikareva, L. M.; Rotov, A. V. *Russ. J. Inorg. Chem. (Engl. Transl.)* **1986**, *31*, 1661–1667. (b) Wayland, B. B.; Newman, A. R. *Inorg. Chem.* **1981**, *20*, 3093–3097. (c) Collman, J. P.; Kim, K. *J. Am. Chem. Soc.* **1986**, *108*, 7847–7849.

(21) Bennett, M. J.; Donaldson, P. B. *J. Am. Chem. Soc.* **1971**, *93*, 3307.

(22) Suzuki, M.; Ishiguro, T.; Kozuka, M.; Nakamoto, K. N. *Inorg. Chem.* **1981**, *20*, 1993–1996.

(23) For an excellent experimental examination of the problems associated with disordered structures, see: Yoon, K.; Parkin, G. *Inorg. Chem.* **1992**, *31*, 1656–1662.

(24) Cotton, F. A.; Wilkinson, G. *Advanced Inorganic Chemistry*, 5th ed.; Wiley: New York, 1988; p 559.

(25) (a) Lawson, H. J.; Atwood, J. D. *J. Am. Chem. Soc.* **1989**, *111*, 6223–6227. (b) Otsuka, S.; Nakamura, A.; Tatsuno, Y.; Miki, M. *J. Am. Chem. Soc.* **1972**, *94*, 3761. (c) Hatward, P. J.; Blake, D. M.; Wilkinson, G.; Nyman, C. *J. Am. Chem. Soc.* **1970**, *92*, 5873. (d) Otsuka, S.; Nakamura, A.; Tatsuno, Y. *J. Am. Chem. Soc.* **1969**, *91*, 6994.

(26) Klingert, B.; Werner, H. *Chem. Ber.* **1983**, *116*, 1450–1462.

(27) PhNO displacement by $PPh_3$ has been observed for RhCl(COD)(PhNO): Vasapollo, G.; Giannoccaro, P.; Allegretta, F. *J. Organomet. Chem.* **1984**, *270*, 111.

(28) Astruc, D.; Hamon, J.; Roman, E.; Michaud, P. *J. Am. Chem. Soc.* **1981**, *103*, 7502–7514.

(29) Miguel-Garcia, J. A.; Maitlis, P. M. *J. Chem. Soc., Chem. Commun.* **1990**, 1472–1473.

(30) See ref 1 and references cited therein.

**Scheme III**

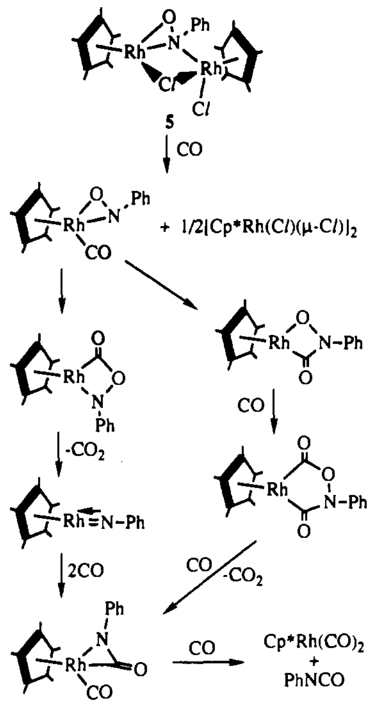

Cp*Rh(NPh). The analogous Ir complex reacts with CO to form an isocyanate complex.[31] This is also expected with the Rh imido complex. With either pathway the isocyanate complex is the immediate precursor to free PhNCO. The expected Rh product from PhNO displacement by CO, Cp*Rh(CO)$_2$, is observed in the reaction mixtures. Unfortunately, the chemistry is more complex than our scheme would indicate, and other, unidentified, Rh products are detected in the mixtures with less than 40% of the nitrogen containing products identified.

The nitrosobenzene salt **6** reacts with CO much more readily probably due to the higher susceptibility to nucleophilic attack resulting from the positive charge and the probable weak PhNO bridge. The reaction pathway to isocyanate is probably the same as that for **5** with rupture of the dimer to the same Cp*Rh(PhNO) fragment. Indeed, the yield of PhNCO is comparable. Cp*Rh(CO)$_2$ is again expected and found.

We had expected **7** to be a good source of PhNCO since there is the possibility of forming two Cp*Rh(PhNO) fragments. The reaction might also be expected to be cleaner since there are no chlorides and only one likely Rh-containing product, Cp*Rh(CO)$_2$. The second idea apparently is valid, and only one metal complex, Cp*Rh(CO)$_2$, is formed; however, no PhNCO is produced. Since higher temperatures had to be used for the CO reaction with **7**, it is possible that secondary reactions of PhNCO give other products which we did not detect.

## Experimental Section

**General Procedures.** All experiments were performed under a dinitrogen atmosphere in a VAC drybox or by Schlenk techniques. Pressure reactions were conducted in a Fischer & Porter pressure bottle. Solvents were carefully dried under dinitrogen by recommended published techniques.[32] Na(Hg)[33] and [Cp*Rh(μ-Cl)Cl]$_2$[34] were prepared as described in the literature. TlBF$_4$ was prepared by the addition of solid Tl$_2$CO$_3$ to 50% HBF$_4$ followed by washing of the precipitated product with a minimum of cold water. The nitrosobenzene, triphenyl phosphine, and trimethyl phosphine (1 M solution in toluene) were used as received (Aldrich). CP grade CO (Matheson) was used. NMR shifts are reported in ppm referenced to TMS for $^1$H and $^{13}$C and to external H$_3$PO$_4$ for $^{31}$P. Microanalyses were performed (drybox) by Oneida Research Services, Inc. HPLC analyses were performed on MeOH quenched (10-to-1) reaction mixtures using a 25 cm, C$_{18}$ reversed-phase microsorb column with 60/40 or 80/20 MeOH/H$_2$O mixtures containing 0.1% nitric acid and a fixed wavelength (254 nm) detector. Yields are based on calibration curves obtained from authentic samples.

**[Cp*Rh(μ-Cl)]$_2$ (1).** To a red solution of [Cp*Rh(μ-Cl)Cl]$_2$ (800 mg, 1.29 mmol) in 30 mL of methylene chloride was added excess Na/Hg (37 g–0.4%, 6.45 mmol). After vigorous stirring for 3.5–5 h, the blue solution was filtered and the solution volume was reduced in vacuo. (Completion of reaction can be determined by $^1$H NMR spectroscopy in CD$_2$Cl$_2$: $\delta$ 1.73, Cp*, [Cp*Rh(μ-Cl)]$_2$; $\delta$ 1.55, Cp*, [Cp*Rh(μ-Cl)Cl]$_2$; see Results). The concentrated solution was layered with hexane and cooled to –40 °C, and 528 mg (0.97 mmol, 75%) of blue-black crystals of **1** were isolated. $^1$H NMR (90 MHz, C$_6$D$_6$) $\delta$ 1.59.

*Caution*: Although we have not experienced any problems with the use of dilute amalgams in CH$_2$Cl$_2$, this is a potential hazard and adequate precautions should be taken. The use of more concentrated amalgams with CH$_2$Cl$_2$ is not recommended.

**[(Cp*Rh)$_2$(μ-Cl)(μ,η$^1$:η$^2$-O$_2$)Cl] (2).** Dry O$_2$ (1 mL, 0.04 mmol) was injected through a rubber septum into a blue CD$_2$Cl$_2$ (0.5 mL) solution of [Cp*Rh(μ-Cl)]$_2$ (20 mg, 0.037 mmol) in a 5 mm NMR tube at –70 °C. With slight warming and shaking, the solution turned red. Variable-temperature $^1$H NMR spectra were then recorded starting with the probe at –70 °C (see Results). The yield was quantitative by NMR.

Complex **2** was prepared on a larger scale for isolation by bubbling O$_2$ (1 atm) into a CH$_2$Cl$_2$ solution of [Cp*Rh(μ-Cl)]$_2$ at –78 °C. When the solution had turned red the volatiles were removed in vacuo (12 h) at –78 °C. The resulting red solid was warmed to ambient temperatures under a dynamic vacuum. In solution, the complex must be kept below ca. –15 °C to avoid decomposition. The stability of the isolated solid was checked by preparing a CD$_2$Cl$_2$ NMR sample at –78 °C. IR (mineral oil) 812 cm$^{-1}$ m ($\nu_{O-O}$). $^1$H NMR (90 MHz, CD$_2$Cl$_2$, –80 °C); $\delta$ 1.70 and 1.55 (s, 30, Cp*). Raising the temperature causes coalescence of the two peaks ($T_c \sim -45$ °C; $\Delta G^\ddagger \sim 50$ kJ/mol). $^{18}$O$_2$ (CIL, 97–98%) labeled **2** was prepared by the following procedure. A solution of [Cp*Rh(μ-Cl)]$_2$ in methylene chloride was subjected to three freeze–pump–thaw cycles on a high vacuum line. Approximately 3 equiv of $^{18}$O$_2$ were injected into the evacuated flask with the solution cooled to –78 °C. With stirring and slight warming, the blue solution turned red and was worked up as described above. IR (mineral oil): 768 cm$^{-1}$.

**Observation of Cp*Rh(O$_2$)(PPh$_3$) (3).** A 0.3-mL solution of PPh$_3$ (20 mg, 0.076 mmol) in CH$_2$Cl$_2$ was injected into a 5-mm, dioxygen free, NMR tube containing **2** (21 mg, 0.037 mmol) dissolved in 0.5 mL of CH$_2$Cl$_2$ at –78 °C. The color of the solution immediately turned green, and with warming to –40 °C, the color returned to red. Low-temperature NMR spectroscopy showed the formation of **3** along with the second product, Cp*RhCl$_2$(PPh$_3$). The formation of **3** is hindered by the presence of excess O$_2$. Complex **3** is unstable in solution above ca. –10 °C. $^1$H NMR (90 MHz, CD$_2$Cl$_2$, –40 °C): $\delta$ 1.56 (d, $J_{HP}$ = 2.4 Hz, 15, Cp*); also phenyl peaks. $^{31}$P NMR (36 MHz, CD$_2$Cl$_2$, –40 °C): $\delta$ 31.0 (d, $J_{PRh}$ = 184 Hz, 1, PPh$_3$).

**[(η$^4$-C$_5$Me$_4$CH$_2$)Rh(PMe$_3$)$_3$]Cl (4).** PMe$_3$ (0.66 mL, 0.66 mmol 1 M in toluene) was injected into a solution of **2** (64 mg, 0.11 mmol) in 5 mL of methylene chloride at –78 °C. The resulting brown solution was warmed to 25 °C under N$_2$. The volatiles were then removed in vacuo, and the residue was dissolved in a minimum volume of CH$_2$Cl$_2$. Layering the solution with ether and cooling to –40 °C gave 75 mg (0.15 mmol, 68%) of brown crystals of **4** after filtration and washing with ether. $^{13}$C{$^1$H} NMR (22.5 and 75 MHz, CD$_2$Cl$_2$, 25 °C): $\delta$ 155.1 (s, CH$_2$=*C*(CMe)$_4$), 104.1 (d, br, $J_{CRh}$ = 4 Hz, CH$_2$=C(*C*Me)$_4$), 102.6 (d, $J_{CRh}$ = 5.4 Hz, CH$_2$=C(*CMe*)$_4$), 73.4 (d, $J$ = 7.6 Hz, *C*H$_2$=C(CMe)$_4$), 18.0-16.0 (br, PMe$_3$), 17.3 (t, $J_{CP}$ = 16.9 Hz, CH$_2$=C(C*Me*)$_4$), 12.0 (d, $J_{CP}$ = 13.6 Hz, CH$_2$=C(C*Me*)$_4$). At –50 °C (internal ring carbons are unchanged): $\delta$ 72.2 (d, br, $J$ = 15.4 Hz, *C*H$_2$=C(CMe)$_4$), 19.5 (t, $J_{CP}$ = 13.9 Hz, PMe$_3$), 16.6 (t, $J_{CP}$ = 17.1 Hz, CH$_2$=C(C*Me*)$_4$), 13.2 (d, $J_{CP}$ = 22.6 Hz, PMe$_3$), 11.7 (d, $J_{CP}$ = 15.2 Hz, CH$_2$=C(C*Me*)$_4$). Assignments were confirmed by DEPT experiment. $^{31}$P NMR (36 MHz, CD$_2$Cl$_2$, –70 °C); –15.8 (dd, $J_{PRh}$ = 127 Hz, $J_{PP}$ = 19.5 Hz, 2, PMe$_3$), –32.2 (dt, $J_{PRh}$ = 164 Hz, $J_{PP}$ = 19.5 Hz, 1, PMe$_3$′). As the temperature is raised the signals collapse and coalesce ($T_c \sim 0$ °C).

**[(Cp*Rh)$_2$(μ-Cl)(μ,η$^1$:η$^2$-PhNO)Cl] (5).** Nitrosobenzene (49 mg—97%, 0.44 mmol) dissolved in 2 mL of methylene chloride was added to a

---

(31) Glueck, D. S.; Wu, J.; Hollander, F. J.; Bergman, R. G. *J. Am. Chem. Soc.* **1991**, *113*, 2041–2050. Glueck, D. S.; Hollander, F. J.; Bergman, R. G. *J. Am. Chem. Soc.* **1989**, *111*, 2719–2721.

(32) Burfield, D. R.; Lee, K.-H.; Smithers, R. H. *J. Org. Chem.*, **1977**, *42*, 3060–3065.

(33) Templeton, J. L.; McCarley, R. E. *Inorg. Chem.* **1978**, *17*, 2293–2299.

(34) Kang, J. W.; Moseley, K.; Maitlis, P. M. *J. Am. Chem. Soc.* **1969**, *91*, 5970–5977.

stirred solution of $[Cp^*Rh(\mu\text{-}Cl)]_2$ (**1**) (239 mg, 0.44 mmol) in 12 mL of toluene. The resultant dark red solution was stirred for 6 h, filtered, and concentrated in vacuo. After the addition of hexane and cooling at –40 °C, dark red crystals of **5** were obtained (216 mg, 0.33 mmol, 75%). IR (mineral oil): 986 $cm^{-1}$ m ($\nu_{NO}$). $^1H$ NMR (300 MHz, $CDCl_3$): $\delta$ 8.64 (d, $J$ = 8.2 Hz, 1, ortho phenyl), 7.54 (d, $J$ = 7.9 Hz, 1, ortho phenyl), 7.28–7.15 (m, 2, meta phenyl), 6.91 (t, $J$ = 7.2 Hz, 1, para phenyl), 1.41 (s, 15, Cp*), 1.37 (s, 15, Cp*). $^{13}C$ (75 MHz, $CDCl_3$): $\delta$ 157.9 (s, ipso phenyl), 127.4 (s, meta or ortho phenyl), 127.2 (s, meta or ortho phenyl), 122.9 (s, meta or ortho phenyl), 122.5 (s, meta or ortho phenyl), 119.3 (s, para phenyl), 92.7 (d, $J$ = 8.5 Hz, $\mathit{C}_5Me_5$), 90.5 (d, $J$ = 8.6 Hz, $\mathit{C}_5Me_5$), 8.9 and 8.6 (s, $C_5\mathit{Me}_5$). Anal. Calcd (found) for $C_{26}H_{35}Cl_2NORh_2$: C, 47.73 (48.15); H, 5.39 (5.53); N, 2.14 (2.08).

**$[(Cp^*Rh)_2(\mu\text{-}Cl)(\mu,\eta^2{:}\eta^2\text{-}PhNO)]BF_4$ (6).** A mixture of $[(Cp^*Rh)_2(\mu\text{-}Cl)(\mu,\eta^1{:}\eta^2\text{-}PhNO)Cl]$ (**5**) (90 mg, 0.14 mmol) and finely powdered $TlBF_4$ (45 mg, 0.15 mmol) was stirred for 4 h in 12 mL of THF. The solution volume was reduced to 4 mL, and the red precipitate was filtered, washed with ether, and dried. The resulting red powder was dissolved in $CH_2Cl_2$, filtered, and layered with ether. Cooling at –40 °C afforded 64 mg (0.091 mmol, 64%) of **6** as red crystals. $^1H$ NMR (300 MHz, $CDCl_3$): $\delta$ 7.55–7.40 (br, 4, phenyl), 7.23 (t, $J$ = 7.4, para phenyl), 1.47 (s, 30, Cp*). $^{13}C$ NMR (75 MHz, $CDCl_3$): $\delta$ 149.9 (s, ipso phenyl), 129.4 (s, meta or ortho phenyl), 125.8 (s, meta or ortho phenyl), 93.2 (d, $J$ = 8.4 Hz, $\mathit{C}_5Me_5$), 8.9 (s, $C_5\mathit{Me}_5$).

**$[(Cp^*Rh)(\mu,\eta^1{:}\eta^2\text{-}PhNO)]BF_2$ (7).** To a stirred mixture of **5** (150 mg, 0.23 mmol), nitrosobenzene (74 mg, 0.69 mmol), and Na/Hg (2.8 g, 0.4%, 0.48 mmol) in 12 mL of THF was added $TlBF_4$ (74 mg, 0.253 mmol). A red intermediate precipitated and redissolved. After 5 h the solution was filtered and the volatiles were removed in vacuo. The residue was washed with hexane, extracted into toluene, and filtered and hexane added to the filtrate. After cooling at –40 °C, dark red crystals of **7** were isolated (109 mg, 0.16 mmol, 69%) after washing with hexane and drying in vacuo. IR (mineral oil): 1001 $cm^{-1}$ m ($\nu_{NO}$). $^1H$ NMR (300 MHz, $CDCl_3$): $\delta$ 7.32–7.19 (m, 4, phenyl), 6.88 (t, $J$ = 7.8 Hz, 1, para phenyl), 1.22 (s, 30, Cp*). $^{13}C$ NMR (75 MHz, $CDCl_3$): $\delta$ 158.3 (s, ipso phenyl), 127.8 (s, meta or ortho phenyl), 127.6 (s, meta or ortho phenyl), 121.7 (s, meta or ortho phenyl), 121.3 (s, meta or ortho phenyl), 115.5 (s, para phenyl), 89.4 (d, $J$ = 8.8 Hz, $\mathit{C}_5Me_5$), 8.4 (s, $C_5\mathit{Me}_5$). Anal. Calcd (found) for $C_{32}H_{40}N_2O_2Rh_2$: C, 55.66 (55.28); H, 5.83 (5.24); N, 4.06 (3.44).

**CO Reactions with 5–7.** These reactions were conducted in a glass Fischer & Porter bottle pressurized to 40 psi of CO with stirring using 20 mg of sample dissolved in $CH_2Cl_2$ (1.5 mL). The reaction with **5** was run for 1.5–2 h with a color change from dark red to a light red. The addition of CO to **6** brought about an immediate color change from red to golden brown and the reaction was run for 30 min. The solution of **7** was stirred overnight under CO at 40 °C with no apparent color change from the dark red of **7**. In each case, at the end of the reaction time the vessel was depressurized and immediately transferred to the drybox for analysis.

PhNCO yields were determined by FTIR spectroscopy (standard curve was prepared using known solutions of PhNCO). Yields of PhNCO: **5**, 35%; **6**, 30%; **7**, 0%. PhNCO yields (as the carbamate, PhNHCOOMe) were confirmed and diphenylurea yields determined from HPLC analysis of MeOH quenched samples. Only traces of urea were found in each case.

IR analysis of the $CH_2Cl_2$ reaction mixtures in the $\nu_{CO}$ region: **5**, 2068, 2055, 1991, and 1826 $cm^{-1}$ and bands for $Cp^*Rh(CO)_2$, at 2018 and 1951 $cm^{-1}$; **6**, 2089, 2064, and 1874 $cm^{-1}$ and bands for $Cp^*Rh(CO)_2$; **7**, no other bands except those for $Cp^*Rh(CO)_2$.

$^1H$ NMR (90 MHz, $CDCl_3$) analysis of reaction mixture nonvolatiles: **5**, $\delta$ 2.05 ($Cp^*Rh(CO)_2$), 1.86, 1.72, 1.62 ($[Cp^*Rh(\mu\text{-}Cl)Cl]_2$), and 1.45; **6**, $\delta$ 2.05 ($Cp^*Rh(CO)_2$), 1.93, 1.68, and 1.42; **7**, $\delta$ 2.05 ($Cp^*Rh(CO)_2$).

**Structure Analyses.** Crystals of **1** and **5** were selected in air, mounted on a glass fiber, and coated with epoxy. Crystals of **4**$\cdot CH_2Cl_2$ and **6**$\cdot 0.5CH_2Cl_2$ were selected while submerged in oil, mounted on a glass fiber, and immediately transferred to the cold stream on the diffractometer. A summary outline of crystallographic and data collection parameters is given in Table I. Details of the data collection and reduction and the structure solution and refinement are provided as supplementary material.

**Acknowledgment.** We thank ARCO Chemical Co., Johnson Matthey (loan of $RhCl_3$), and the Division of Chemical Sciences, Office of Basic Energy Sciences, Office of Energy Research, U.S. Department of Energy (Grant No. DE-FG02-88ER13880), for support of this work. The National Science Foundation provided a portion of the funds for the purchase of the X-ray (CHE-9011804) and NMR (PCM-8115599 and CHE 89-08304) equipment.

**Supplementary Material Available:** Additional ORTEP diagrams (see text) and tables of detailed X-ray experimental data, positional parameters, thermal parameters, bond distances and angles, and least squares planes (34 pages). Ordering information is given on any current masthead page.